ACS APPLIED MATERIALS & INTERFACES

RESEARCH ARTICLE

www.acsami.org

Synthesis of Biocompatible, Mesoporous Fe_3O_4 Nano/Microspheres with Large Surface Area for Magnetic Resonance Imaging and Therapeutic Applications

Shouhu Xuan,[†,‡] Feng Wang,[†] Josie M. Y. Lai,[§] Kathy W. Y. Sham,[§] Yi-Xiang J. Wang,[⊥] Siu-Fung Lee,[†] Jimmy C. Yu,[†] Christopher H. K. Cheng,[§] and Ken Cham-Fai Leung*[,†]

[†]Center of Novel Functional Molecules and Institute of Molecular Functional Materials, Department of Chemistry, [§]School of Biomedical Sciences, and [⊥]Department of Imaging and Interventional Radiology, Prince of Wales Hospital, The Chinese University of Hong Kong, Shatin, NT, Hong Kong SAR, People's Republic of China

[‡]CAS Key Laboratory of Mechanical Behavior and Design of Materials, Department of Mechanics and Mechanical Engineering, The University of Science and Technology of China, Hefei 230026, People's Republic of China

Supporting Information

ABSTRACT: This article reports the fabrication of mesoporous Fe_3O_4 nano/microspheres with a high surface area value (163 m^2/g, Brunauer–Emmett–Teller) and demonstrates their use for drug loading, release, and magnetic resonance imaging (MRI). These monodispersed, mesoporous Fe_3O_4 nano/microspheres with controllable average sizes ranging from 50 to 200 nm were synthesized using a Fe_3O_4/poly(acrylic acid) hybrid sphere template and subsequent silica shell formation and removal. We found that the SiO_2 coating is a crucial step for the successful synthesis of uniform mesoporous Fe_3O_4 nano/microspheres. The as-synthesized mesoporous Fe_3O_4 nanospheres show a high magnetic saturation value (M_s = 48.6 emu/g) and could be used as MRI contrast agents (r_2 = 36.3 s^{-1} mM^{-1}). Trypan blue exclusion and MTT assay (see Supporting Information) cytotoxicity analyses of the nanospheres based on HepG2 and MDCK cells showed that the products were biocompatible, with a lower toxicity than lipofectamine (positive control). Hydrophilic ibuprofen and hydrophobic zinc(II) phthalocyanine drug loading into mesoporous Fe_3O_4 nanospheres and selected release experiments were successfully achieved. The potential use of mesoporous Fe_3O_4 nanospheres in biomedical applications, in light of the nano/microspheres' efficient drug loading and release, MRI, and low cytotoxicity, has been demonstrated. It is envisaged that mesoporous Fe_3O_4 nanospheres can be used as drug carriers and MRI contrast agents for the reticuloendothelial system; they can also be delivered locally, such as via a selective catheter.

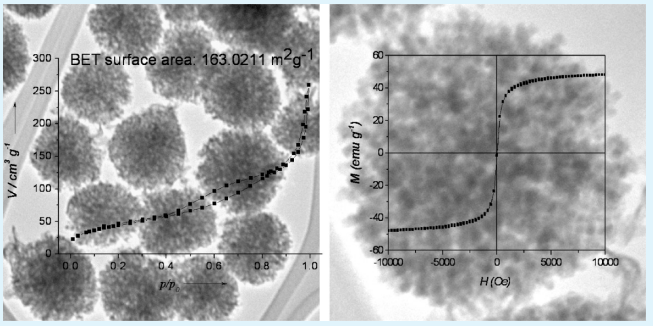

KEYWORDS: contrast agent, iron oxide, magnetic resonance imaging, mesoporous materials, targeted drug delivery

1. INTRODUCTION

Owing to their specific functional characteristics and importance in a wide variety of technical applications, Fe_3O_4 nano- and microspheres have been investigated extensively as ferrofluids, colored pigments, high-density magnetic recording media, chemical sensors, electrophotographic developers and theranostic materials in biological areas.[1−9] The effectiveness of Fe_3O_4 in these fields depends on the particles' specific composition, crystallinity, mesoporosity, surface properties, morphology, and texture. Therefore, the design and synthesis of various magnetic Fe_3O_4 nanoarchitectures, such as particles, spheres, flowers, wires, tubes, and mesoporous structures, had drawn a lot of attention in recent years.[10−20]

Among various reported morphologies, mesoporous Fe_3O_4 nanospheres are of great interest because of their large surface areas and well-defined tunable pore structures and sizes.[21−27] In order to explore their biomedical applications, such as selective biomolecular separation, drug delivery, and cell imaging, recently, mesoporous materials, combined with other properties, demonstrated great prospects in imaging, diagnosis, and therapy.[28−30] Magnetic nanomaterials (Fe_3O_4 and γ-Fe_2O_3) show good implications in drug delivery with in vivo locoregional magnetic targeting. Noncytotoxic, relatively large (>20 nm) nano/microspheres will be quickly taken up by the reticuloendothelial system (RES).[31] This allows targeted delivery of these nano/microspheres to the liver, spleen, lymph nodes, and bone marrow,[31−33] functioning either as a MRI contrast agent or as a drug carrier. Targeted delivery can be further improved by locoregional

Received: September 14, 2010
Accepted: December 22, 2010
Published: January 13, 2011

magnetic targeting.[34] Alternatively, these nano/microspheres as drug carriers can also be delivered intraarterially via a superselectively placed catheter, whereas regional retention of drugs can be enhanced by a locoregional magnetic field. These nanomaterials can encapsulate specific drugs to the designated target organs or lesions inside the body, without any premature drug release. This can facilitate its therapeutic efficiency and avoid damaging to healthy organs or tissues because of drug toxicity.[35] Furthermore, the magnetic particles could be used as T_2 contrast agents in magnetic resonance imaging (MRI) and magnetic hyperthermia, allowing better diagnosis and cancer treatment.[36−43] In this context, magnetic mesoporous nanomaterials with magnetic properties would have great potential for simultaneous imaging, magnetic hyperthermia, and drug delivery.

The spherelike mesoporous Fe_3O_4 nanomaterials have shown highly promising biological applications. During the past decades, mesoporous Fe_3O_4 nanospheres with tunable pore sizes have been synthesized using different strategies such as the hydrothermal method, precursor synthesis, and a self-assembly process.[13,18,44−46] For any mesoporous Fe_3O_4 materials used in biological applications, the particles should possess uniform particle sizes, large surface areas, and biocompatible surfaces. However, the Brunauer−Emmett−Teller (BET) areas of the previously reported Fe_3O_4 materials are always smaller than 100 m^2/g. Their corresponding cytotoxicities were not investigated as well.[44−46] Preparation of biocompatible mesoporous Fe_3O_4 materials remains a challenge.

In this work, fabrication of mesoporous Fe_3O_4 nanospheres, drug release, and MRI are reported. Poly(acrylic acid) (PAA)-entangled Fe_3O_4 nanospheres (Fe_3O_4/PAA) were synthesized, followed by formation of the SiO_2 layer onto the surface of Fe_3O_4/PAA nanospheres. The resultant products were core/shell-like nanostructures. After decomposition of the PAA polymer using a vacuum thermal treatment, followed by etching of the SiO_2 layer, mesoporous Fe_3O_4 nanospheres were successfully synthesized. The size of these mesoporous Fe_3O_4 nano/microspheres was tunable, from 50 to 200 nm. The drug release and MRI properties were also investigated. In addition, trypan blue exclusion and MTT assay (see Supporting Information) cytotoxicity analyses based on HepG2 and MDCK cells were studied for biocompatibility of the nanospheres. The efficient drug loading and release, MRI, and low cytotoxicity analysis of the product render them useful in biomedical applications.

2. EXPERIMENTAL SECTION

Materials. Ferric chloride hexahydrate ($FeCl_3 \cdot 6H_2O$), sodium acetate (NaOAc), sodium acrylate, ethylene glycol (EG), diethylene glycol (DEG), tetraethyl orthosilicate (TEOS), and ibuprofen were obtained from Aldrich. All chemicals were of analytical grade and were used without further purification. Deionized water was obtained from a Barnstead RO pure system and was bubbled with high-purity nitrogen for at least 30 min before use.

Synthesis of Monodispersed, Poly(acrylic acid) (PAA)-Entangled Fe_3O_4 Nano/Microspheres. Monodispersed Fe_3O_4/PAA nano/microspheres with various average sizes were synthesized according to our previous reports.[47−51] For a typical synthesis of 200 nm Fe_3O_4/PAA microspheres, $FeCl_3 \cdot 6H_2O$ (0.54 g), NaOAc (1.5 g), and sodium acrylate (1.5 g) were dissolved in EG (20 mL). After vigorous stirring of the mixture for 1 h, the homogeneous solution was transferred to a Teflon-lined stainless steel autoclave (25 mL volume), sealed, and heated to 200 °C. After a 12 h reaction period, the autoclave was cooled to room temperature. The obtained Fe_3O_4/PAA spheres were washed with water and ethanol and then dispersed in water (15 mL). In this synthesis, the average sizes (20−300 nm) of the Fe_3O_4 nano/microspheres can be controlled by varying the ratio of the solvents (V_{EG}/V_{DEG}) in the system.[52]

Synthesis of Monodispersed, Mesoporous Fe_3O_4 Nano/Microspheres. The obtained Fe_3O_4/PAA spheres were coated by a layer of SiO_2 shell with 25 nm thickness. In particular, an aqueous solution (2.5 mL) of Fe_3O_4/PAA was diluted with water (0.5 mL) and ethanol (30 mL). The mixture was homogenized by ultrasonication for 30 min, prior to the addition of an ammonia solution (1 mL). After 30 min, a solution of TEOS (0.1 mL) in ethanol (5 mL) was injected into the solution. The reaction was performed for 100 min, and the product was collected with the help of a magnet and then washed several times with ethanol and water. Finally, the product was dried in a vacuum for 12 h to obtain the Fe_3O_4/PAA@SiO_2 core/shell nanospheres. The as-synthesized Fe_3O_4/PAA@SiO_2 nanospheres were transformed into the corresponding mesoporous Fe_3O_4@SiO_2 nanospheres by thermal treatment. Typically, Fe_3O_4/PAA@SiO_2 nanospheres were heated in a vacuum with a heating rate of 5 °C/min. After treatment at 500 °C for 6 h, the product was cooled to room temperature to give the product mesoporous Fe_3O_4@SiO_2 nanospheres. Subsequently, the spheres were redispersed in an aqueous NaOH solution (0.5 M) for 6 h under mechanical stirring in order to dissolve the silica shell. The particles were collected by magnetic separation and washed several times with water and ethanol. The residue was dried to yield the porous Fe_3O_4 nano/microspheres. The porous Fe_3O_4 nano/microspheres were stable and could be well dispersed in water and cell culture medium.

Characterization. Powder X-ray diffraction (XRD) patterns of the products were obtained on a Bruker D8 Advance diffractometer equipped with graphite-monochromatized Cu Kα radiation (λ = 1.5406 Å). Transmission electron microscopy (TEM) photographs were recorded on a FEI CM120 microscope at an accelerating voltage of 120 kV and on a high-resolution transmission electron microscope (Tecnai F20, FEI) at an accelerating voltage of 200 kV. The general morphology of the product was characterized by scanning electron microscopy (SEM; FEI Quanta 400 FEG microscopes). IR spectra were recorded in the wavenumbers ranging from 4000 to 500 cm^{-1} with a Nicolet model 759 Fourier Transform infrared (FTIR) spectrometer using a KBr wafer. The magnetic properties ($M-H$ curve) were measured at room temperature on a Lakeshore 7300 vibrating sample magnetometer. The iron concentration was determined using inductively coupled plasma optical emission spectroscopy on an Optima 4300 DV inductively coupled plasma optical emission spectrometer. Samples were dissolved in a 2% HCl solution with a few drops of a $SnCl_2$ solution. Iron absorption was observed at 238.204 nm and calibrated with standard solutions. The BET surface areas of the samples were analyzed by nitrogen adsorption−desorption isotherm measurements at 77 K on a nitrogen adsorption apparatus (Micromeritics ASAP 2010). All of the samples were degassed at 150 °C prior to nitrogen adsorption measurements. Pore size distributions were calculated from the desorption branch of the isotherm by the Barrett−Joyner−Halenda (BJH) method using the Halsey equation.

MR Relaxometry. For MRI, the capability of nanospheres to influence the T_2 relaxation time was studied using a clinical 1.5 T whole-body MR system (Sonata, Siemens Symphony, Erlangen, Germany) with a standard human knee radio-frequency coil for excitation and signal reception. For MR measurements, nanospheres were diluted in distilled water at iron concentrations of 100, 10, 5, 2.5, 1, and 0.5 μg/mL. The imaging sequence was a standard Carr−Purcell−Meiboom−Gill pulse sequence with the following parameters: time of repetition = 2000 ms, time of echo (TE) range = 30−960 ms, 32 echoes, field of view = 134 × 67 mm^2, matrix = 128 × 64, slice thickness = 5 mm, and number of excitations = 3. T_2 relaxation times were calculated by a linear fit of the logarithmic ROI signal amplitudes versus TE. The T_2 relaxivity (r_2) was

Scheme 1. Graphical Representation of the Fabrication of Mesoporous Fe_3O_4 Nano/Microspheres with Large Surface Area

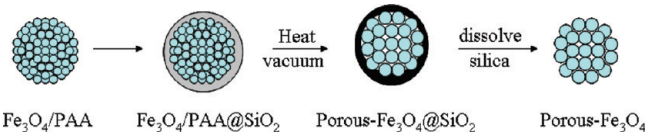

determined by a linear fit of the inverse relaxation times as a function of the iron concentrations used.

Cytotoxicity Assay. For the cell culture, Madin−Darby Canine Kidney (MDCK, ATCC CCL-34) cells were grown in a DMEM medium supplemented with 10% FBS, 100 g/mL streptomycin, and 50 U/mL penicillin at 37 °C in a humidified atmosphere with 5% CO_2. MDCK cells or HepG2 (liver carcinoma) cells were seeded in 24-well plates overnight, at a density of 50 000 cells/well. Because, at any culturing condition, the cell viability is not 100%, a control test without any iron-NP, was always conducted under the same condition. After 24 h of incubation of iron-NP and/or lipofectamine (a positive control), the media were retained from each well, followed by washing with a phosphate-buffered saline (PBS) solution. Then, the cells were trypsinized using 0.15 mL of 0.25% trypsin−ethylenediaminetetraacetic acid (Gibco Invitrogen Co., USA). After the cells have been totally detached from the bottom of each well, all cell suspensions retained in the media were centrifuged at 1500 rpm for 3 min. The cell pellet was resuspended in 0.2 mL of a PBS solution. After staining by trypan blue dye, the cell density was counted using a hemacytometer. The cell viability was then calculated.

Drug Loading. Typically, the mesoporous Fe_3O_4 nanospheres (40 mg) were added into 10 mL of an ibuprofen/hexane solution (150 mg/mL) at room temperature. The mixture was stirred for 24 h, and then the drug-loaded particles were magnetically separated. On the other hand, the mesoporous Fe_3O_4 nanospheres (40 mg) were added into 5 mL of a ZnPC/ethanol solution (1 mM) at room temperature. The mixture was stirred for 24 h, and then the drug-loaded particles were magnetically separated.

3. RESULTS AND DISCUSSION

The fabrication of porous Fe_3O_4 nano/microspheres is outlined in Scheme 1. PAA-entangled Fe_3O_4 nano/microspheres (Fe_3O_4/PAA) were prepared by using a hydrothermal method.[47−52] Because each sphere was composed of many tiny primary nanocrystals (nanograins) that were entangled with PAA polymers, these Fe_3O_4/PAA spheres retained superparamagnetic behavior at room temperature. The as-prepared Fe_3O_4/PAA spheres were coated with a SiO_2 layer by a modified sol−gel process to give Fe_3O_4/PAA@SiO_2 spheres. Then, a thermal treatment in a vacuum was facilitated for decomposition of the PAA polymer of Fe_3O_4/PAA@SiO_2 spheres, yielding the mesoporous Fe_3O_4@SiO_2 core/shell structures. Finally, the SiO_2 layer of the mesoporous Fe_3O_4@SiO_2 spheres was etched away with a NaOH solution. Afterward, mesoporous Fe_3O_4 nano/microspheres that possess large surface areas were successfully synthesized. Because the Fe_3O_4/PAA nano/microspheres could be synthesized with tunable average sizes[37,38] ranging from 6 to 300 nm, eventually, the resulting 6−300 nm porous Fe_3O_4 nano/microspheres could also be prepared. In this work, however, only the syntheses of 50−200 nm mesoporous Fe_3O_4 nano/microspheres were investigated. Raman spectroscopy has been employed to characterize the mesoporous Fe_3O_4 nano/microspheres (Figure S1 in the Supporting Information).

In order to demonstrate the simplicity of this facile approach, the synthesis of 200 nm mesoporous Fe_3O_4 microspheres with large surface areas was first investigated. Parts a and b of Figure 1 reveal typical SEM images of the as-synthesized, mesoporous Fe_3O_4 microspheres. The average size of the microsphere is approximately 200 nm, and they are free of surface cracks and intersphere adherence. The uniform particle size distribution of the mesoporous Fe_3O_4 microspheres is clearly demonstrated from the TEM images (Figure 1c), which agreed well with the above SEM analysis. From a TEM image of a single particle (inset of Figure 1d), it is clearly revealed that the Fe_3O_4 microsphere is also composed of tiny primary nanocrystals that possess mesopores. The specific surface area and pore volume data of the 200 nm mesoporous Fe_3O_4 microspheres were characterized using the nitrogen sorption technique, with a typical isotherm shown in Figure 2. The isotherm demonstrates a type IV isotherm along with two small, but obvious, hysteresis loops at relative pressures of P/P_0 = 0.45−0.78 and 0.90−0.98, indicating the presence of interparticle and nonordered mesoporosity in the sample.[53,54] Because the primary Fe_3O_4 nanograins are randomly packed, the pore size distribution of the product is not very uniform

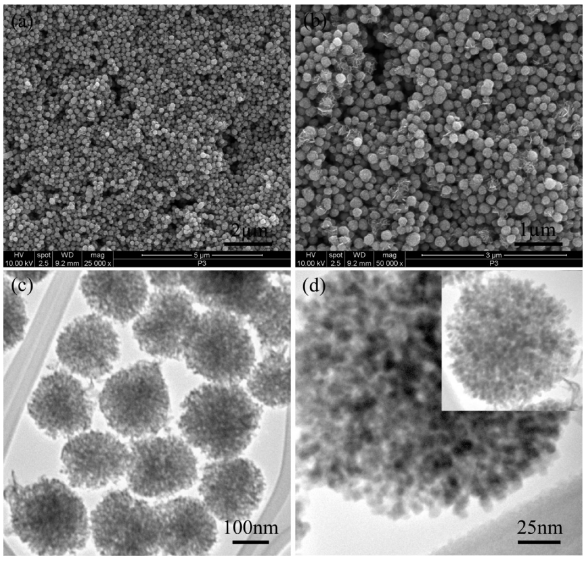

Figure 1. SEM (a and b) and TEM (c and d) images of the as-prepared mesoporous Fe_3O_4 microspheres.

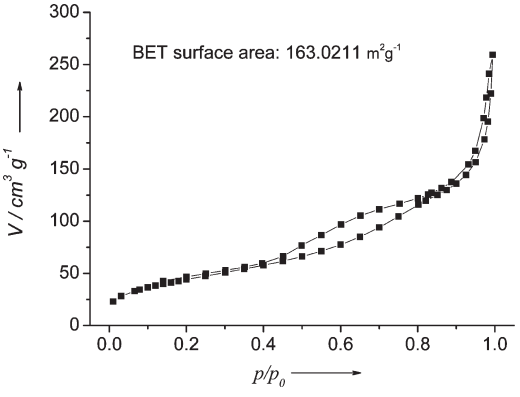

Figure 2. Nitrogen adsorption−desorption isotherm curve of the as-prepared mesoporous Fe_3O_4 nanospheres (V = volume; p = pressure of N_2).

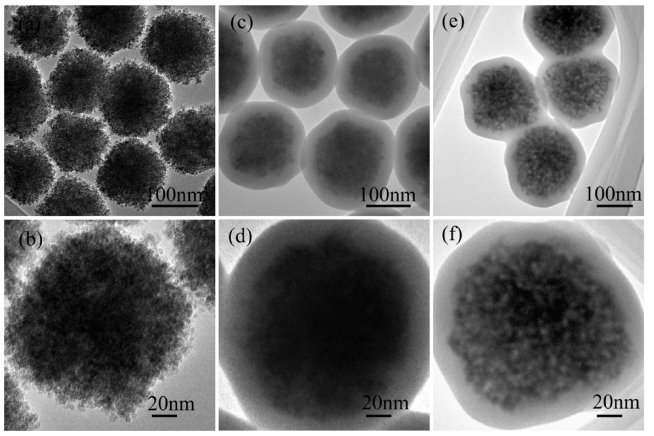

Figure 3. TEM images of the Fe_3O_4/PAA (a and b), Fe_3O_4/PAA@SiO_2 (c and d), and mesoporous Fe_3O_4@SiO_2 (e and f) microspheres.

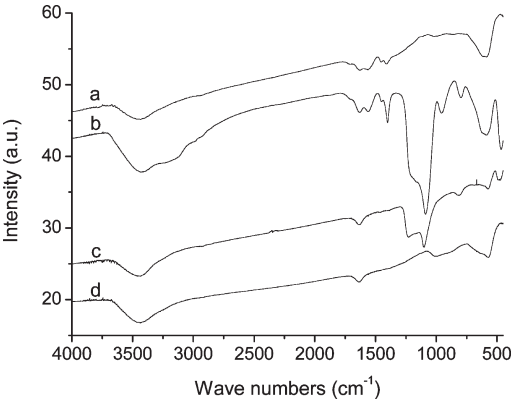

Figure 4. FTIR spectra of the Fe_3O_4/PAA (a), Fe_3O_4/PAA@SiO_2 (b), mesoporous Fe_3O_4@SiO_2 (c), and mesoporous Fe_3O_4 (d) microspheres.

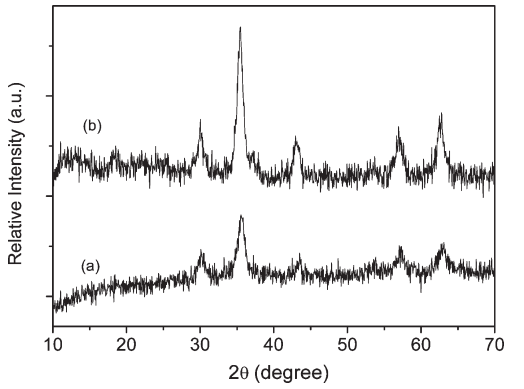

Figure 5. XRD patterns of the Fe_3O_4/PAA (a) and mesoporous Fe_3O_4 (b) microspheres.

(Figure S2 in the Supporting Information). However, a major pore size was found to be 11 nm. The specific surface area was determined to be 163 m^2/g. This value is relatively large compared to other recently reported mesoporous Fe_3O_4 structures, whereas their BET surface areas are typically less than 100 cm^3/g.[44−46] Based on the SEM, TEM, and BET analysis results, our method can be extended to synthesize size-tunable, mesoporous Fe_3O_4 nano/microspheres with large specific surface areas (vide infra).

Detailed synthetic processes of the mesoporous Fe_3O_4 microspheres were performed in order to understand the formation mechanism of the porous products. Because of the strong coordinative effect of the iron carboxylate (FeOOC) moieties, the PAA polymer was uniformly dispersed throughout the whole Fe_3O_4/PAA microsphere cluster, from the surface to the core.[47−52,55] Thermogravimetric analysis (TGA) indicates that the PAA content is approximately 20% by weight in the Fe_3O_4/PAA microspheres (Figure S3a in the Supporting Information). Therefore, such a hybrid microsphere with a large organic component is a suitable precursor for synthesis of the mesoporous Fe_3O_4 with large surface area. Parts c and d of Figure 3 show the typical TEM images of the Fe_3O_4/PAA@SiO_2 microspheres, which clearly indicate the well-defined core/shell nanostructure. The shell thickness can be controlled from several to several hundred nanometers by variation of the TEOS concentration. The Fe_3O_4/PAA@SiO_2 microspheres were calcined at 500 °C in a vacuum for 6 h in order to decompose the organic polymer composition of the hybrid core. As shown in parts e and f of Figure 3, after thermal treatment, the core/shell nanostructure remained in the resulting product mesoporous Fe_3O_4@SiO_2. In comparison to Fe_3O_4/PAA@SiO_2, however, the solid core was transformed into a mesoporous one. The formation of the mesoporous nanostructure might be explained by decomposition of the PAA polymer and fusion of the primary Fe_3O_4 nanograins during vacuum calcination. Figure 4b shows the FTIR spectrum of the Fe_3O_4/PAA@SiO_2 core/shell microspheres. The bands appearing at 580 and 1454 cm^{-1} are related to the Fe−O vibration and the CH_2 bending mode, respectively. The other two absorptions located at 1556 and 1405 cm^{-1} can be attributed to the characteristic bands of the carboxylate groups,[55,56] of the asymmetric and symmetric C−O stretching modes of the COO^- group, respectively. In addition, the characteristic peaks at 1076 and 960 cm^{-1} correspond to the symmetric and asymmetric stretching vibrations of the terminal group in Si−O−R/Si−OH and Si−O−Si bonds. Evidently, all of the CH_2 and carboxylate absorptions have disappeared in the FTIR spectrum of the mesoporous Fe_3O_4@SiO_2 (Figure 4c). Therefore, it is clear that the PAA polymer decomposed during thermal treatment, which led to formation of the mesopores. Finally, the SiO_2 layer of the mesoporous Fe_3O_4@SiO_2 was etched away in a NaOH solution (Figure 4d), to yield the desired mesoporous Fe_3O_4 microspheres with large surface areas. Figure 5b shows the XRD patterns of the as-prepared mesoporous Fe_3O_4, wherein all of the XRD peaks can be indexed to the face-centered-cubic phase of Fe_3O_4 (JCPDS no. 19-0629). Interestingly, in comparison to the Fe_3O_4/PAA hybrid spheres (Figure 5a), the grain size of the mesoporous Fe_3O_4 slightly increased from 7.5 to 8.3 nm (calculated by using the Scherrer equation), which can account for fusion of the nanograins during thermal treatment. Because of decomposition of the PAA polymer and fusion of the primary Fe_3O_4 nanograins, mesoporous Fe_3O_4 microspheres with high BET surface area values were successfully obtained.[53,57]

On the basis of a series of comparable experiments, we found that the SiO_2 coating is a crucial step for the successful synthesis of uniform mesoporous Fe_3O_4 nano/microspheres. Without the SiO_2 coating, large irregular mesoporous Fe_3O_4 particles often existed in the product because of the ripening process between two mesoporous Fe_3O_4 microspheres at high temperature. In addition, the SiO_2 coating can prevent the primary nanograins of

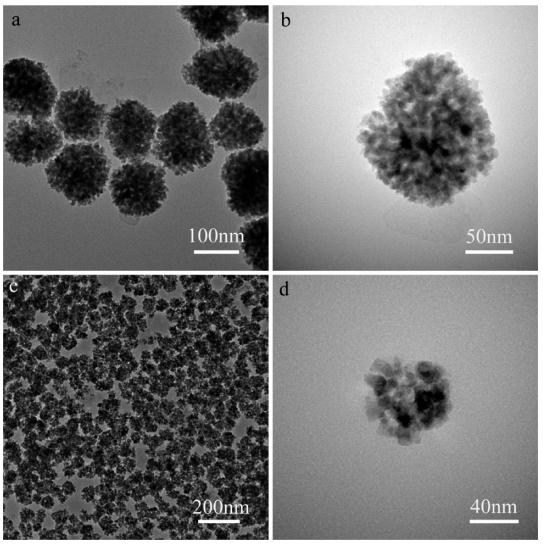

Figure 6. TEM images of the as-prepared mesoporous Fe_3O_4 nano/microspheres with average sizes of 130 nm (a and b) and 60 nm (c and d).

the Fe_3O_4/PAA hybrid spheres from fusing to form large grains during calcination. On the other hand, we use polyaniline as the protecting layer and the grain size of the Fe_3O_4 product is far larger than the one produced under SiO_2 coating (data not shown). Moreover, the SiO_2 coating and etching processes render a high density of hydroxyl groups on the mesoporous microsphere surface and enhance their water dispersity (Figure S4 in the Supporting Information).[57]

This synthetic approach allows facile control over the size of the mesoporous Fe_3O_4 spheres. For comparison, two other mesoporous Fe_3O_4 with average sizes of 130 and 60 nm were fabricated by using Fe_3O_4/PAA hybrid spheres of different sizes as the precursors.[52] Representative TEM images of the resulting 130 and 60 nm mesoporous Fe_3O_4 nano/microspheres are shown in Figure 6. The mesoporous nature of the particles can be observed in parts b and d of Figure 6. Therefore, this method enables the synthesis of a new series of size-controllable, mesoporous Fe_3O_4 nano/microspheres.

The magnetic properties of the mesoporous Fe_3O_4 microspheres have been investigated using a vibrating sample magnetometer. Figure 7 shows the hysteresis loop of typical mesoporous Fe_3O_4 microspheres measured by sweeping the external field between -1 and $+1$ T at room temperature. No obvious remanence or coercivity was observed in the magnetization curve at room temperature, suggesting the soft magnetic character. With the soft magnetic property, capillary blockage by aggregations formed by residual magnetism after removal of the applied field would be avoided. The saturated mass magnetization is estimated to be 48.6 emu/g. Therefore, the as-prepared mesoporous Fe_3O_4 microspheres can be easily separated from the reaction solution by applying a relatively low magnetic field gradient, which renders the particles cost-effective and promising for various applications.

Fe_3O_4 particles are prevalent in molecular imaging as the contrast agents for MRI because of their localized shortening of the spin−spin proton relaxation time.[58] The as-prepared mesoporous Fe_3O_4 microspheres can be used as MRI contrast agents because the product can accelerate the transverse relaxation of water protons. In the present work, transverse (T_2) relaxation times of protons from the dispersion containing mesoporous

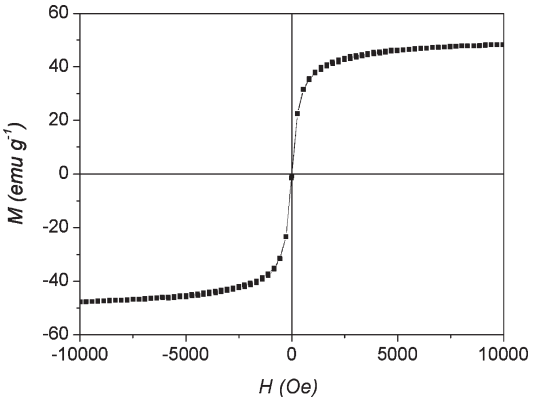

Figure 7. $M-H$ curves of the as-prepared mesoporous Fe_3O_4 microspheres.

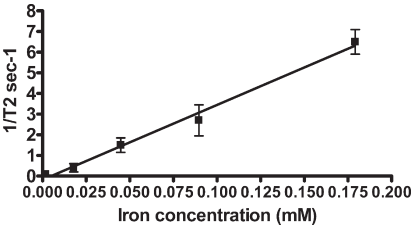

Figure 8. r_2 relaxivity measurement of the mesoporous Fe_3O_4 microspheres.

Fe_3O_4 microspheres were measured and the r_2 relaxivity of the product is 36.3 s^{-1} mM^{-1} Fe (Figures 8 and S5 in the Supporting Information). The relaxivity of our mesoporous Fe_3O_4 particles is close to that of VSOP-C184 and Supravist, which indicates that the as-prepared soft magnetic mesoporous Fe_3O_4 spheres are potential MRI contrast agents. The r_2 relaxivity value of the mesoporous Fe_3O_4 particles is lower than that for the previously reported Fe_3O_4/PAA microspheres, which may be due to their different crystalline nature and chemical environments. In the present work, the Fe_3O_4/PAA microspheres have been treated under SiO_2 coating, thermal treatment, and the SiO_2 etching process, which render the chemical environment of the nanograins (8.3 nm) of the mesoporous Fe_3O_4 microspheres different from the ones of the solid Fe_3O_4/PAA microspheres. The mesoporous Fe_3O_4 microspheres demonstrated a lower r_2 relaxivity than the solid Fe_3O_4 microspheres. That is, the particle's r_2 is also dependent on their crystalline nature and chemical environment. It is reasonable to believe that our current nanoparticle, which contains a non iron oxide void space, decreases its r_2 relaxivity.

In order to achieve biological applications, the ideal materials should be biocompatible. As described above, the mesoporous Fe_3O_4 nanospheres possess good water dispersity, which indicates the potential biosafety of these particles. Photodynamic therapy agent zinc(II) phthalocyanine (ZnPC) molecules were loaded into the mesoporous Fe_3O_4 nanospheres. Phthalocyanine and porphyrin compounds are candidates for photodynamic therapy.[59,60] For cytotoxicity evaluation of the particles, MDCK (kidney) and HepG2 (liver carcinoma) cells represent two different possible detoxification routes of the particles. Trypan blue exclusion assay (Figure 9) and MTT assay (Figure S6 in the Supporting Information) were employed. Parts A and B of Figures 9

reveal respectively the viabilities of liver carcinoma HepG2 cells and MDCK cells, incubated with different concentrations of mesoporous Fe_3O_4/ZnPC nanospheres and 10 nm Fe_3O_4 nanoparticles for 24 h. Trypan blue exclusion assay revealed that the cell viability was not adversely affected (80−90%) of control at concentrations up to 40 μg/mL for both particles. The mesoporous Fe_3O_4/ZnPC showed a little bit higher cell toxicity for HepG2 cells than for MDCK cells. However, in comparison to lipofectamine (positive control), they exhibited a lower cell toxicity, which indicated that the product is biocompatible.

In addition to the practical biological applications of nano/microspheres in MRI, the as-prepared mesoporous Fe_3O_4 nanospheres could be extended to drug delivery. To demonstrate the applicability of this mesoporous magnetic system, we employed the mesoporous Fe_3O_4 nanospheres as a drug carrier for ibuprofen ($C_{13}H_{18}O_2$, MW = 206.28, hydrophilic) and ZnPC ($C_{32}H_{18}N_8Zn$, MW = 579.95, hydrophobic) as the model drugs.

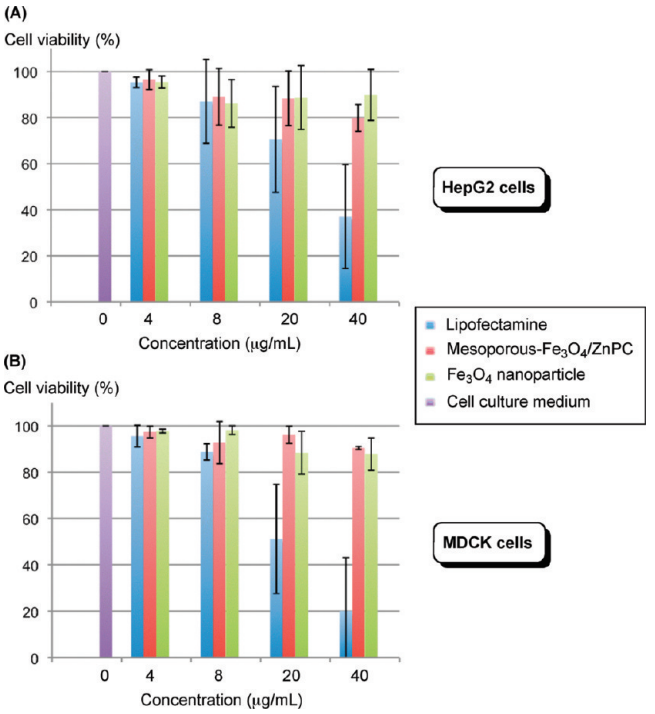

Figure 9. Viability of HepG2 (A) and MDCK (B) cells (%) incubated with lipofectamine, mesoporous Fe_3O_4/ZnPC nanospheres, and 10 nm Fe_3O_4 nanoparticles at different concentrations (μg/mL) with trypan blue exclusion assay.

Drug loading and release experiments of mesoporous Fe_3O_4/ibuprofen nanospheres were performed similarly to the previous report.[45] The capacity of ibuprofen loading of mesoporous Fe_3O_4 nanospheres was approximately 74.5 mg/g, which was obtained from the UV/visible absorbance difference before mesoporous Fe_3O_4 addition and after their removal, as shown in Figure 10b. Figure 10a shows the release profile of ibuprofen in a PBS solution (pH = 7.5) over a 72 h period. The release was relatively fast during the first 20 h but decreased with time and reached a plateau at 81% after 72 h. In addition, photosensitizing molecules ZnPC could be loaded to the as-prepared mesoporous Fe_3O_4 nanospheres to form the mesoporous Fe_3O_4/ZnPC composite spheres. The UV/visible absorbance difference before mesoporous Fe_3O_4 addition and after their removal is shown in Figure 10c. The water-insoluble ZnPC molecules were securely trapped in the pores when the mesoporous Fe_3O_4/ZnPC composite spheres were dispersed in a water or PBS solution. However, ZnPC would be released from the mesoporous Fe_3O_4/ZnPC spheres in ethanol. Eventually, the as-prepared mesoporous Fe_3O_4/ZnPC composite spheres exhibit cytotoxicity under irradiation, which enables the mesoporous Fe_3O_4/ZnPC composite sphere itself to act simultaneously as diagnostic and therapeutic agents. The success of loading and release of both hydrophilic and hydrophobic drugs from mesoporous Fe_3O_4 microspheres will render them effective theranostic materials. It is envisaged that, after intravenous administration, our as-prepared mesoporous Fe_3O_4 nano/microspheres will be quickly taken up by the RES because of their particle sizes.[31] This allows targeted delivery of these Fe_3O_4 nano/microspheres to the liver, spleen, lymph nodes, and bone marrow[31−33] functioning as a MRI contrast agent or as a drug carrier. In the later case, this targeted delivery can be further improved by locoregional magnetic targeting.[34] Alternatively, these Fe_3O_4 nano/microspheres as drug carriers can also be delivered intraarterially via a superselectively placed catheter, and again regional retention can be enhanced by a locoregional magnetic field. An example of such an application with a magnetic targeted carrier bound to doxorubicin (metallic iron-activated carbon doxorubicin) in a human subject has been described.[61]

4. CONCLUSION

Biocompatible, large-surface-area, and soft magnetic Fe_3O_4 nano/microspheres with mesoporous nanostructure have been synthesized successfully via a facile SiO_2 protective templating method. More importantly, the average sizes of these mesoporous Fe_3O_4 nano/microspheres can be controllably obtained from

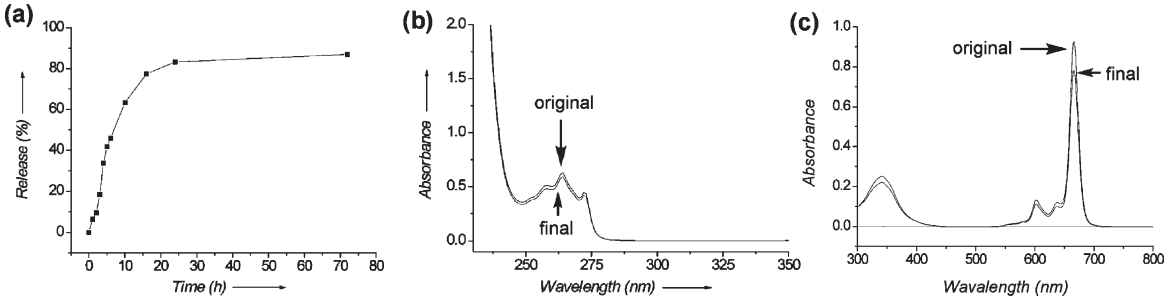

Figure 10. Ibuprofen release profile from mesoporous Fe_3O_4 nanospheres in a PBS (pH = 7.5) solution (a), UV/visible absorption spectra of original and final ibuprofen solutions after being diluted with water (b), and UV/visible absorption spectra of the original and final ZnPC solutions after being diluted with ethanol (c).

50 to 200 nm. TEM images and nitrogen sorption measurement indicated that the mesoporous Fe_3O_4 microspheres have mesoporous structure with a BET surface area of 163 m^2/g. Vibrating sample magnetometry analysis revealed that these particles are soft magnetic without obvious remanence or coercivity. M_s of the product is about 48.6 emu/g, and the r_2 relaxivity is 36.3 s^{-1} mM^{-1} Fe. Trypan blue exclusion and MTT assay cytotoxicity analyses of the nanospheres based on HepG2 and MDCK cells showed that the micro/nanospheres products (with and without ZnPC) were biocompatible, with a lower toxicity than lipofectamine (positive control). Hydrophilic ibuprofen and hydrophobic ZnPC drug loading into the mesoporous spheres and selected release experiments were successfully achieved, indicating that the mesoporous Fe_3O_4 nano/microspheres can be potentially used for drug delivery. As a result, these multifunctional biocompatible mesoporous Fe_3O_4 nano/microspheres are potential theranostic materials for simultaneous MRI and drug delivery. It is envisaged that the mesoporous Fe_3O_4 nanospheres can be used as drug carriers or MRI contrast agents for RES; they can also be delivered locally, such as via a selective catheter.

■ ASSOCIATED CONTENT

Supporting Information. BJH pore size data, Raman spectroscopic data, TGA, magnetic separation, and MRI of the spheres. This material is available free of charge via the Internet at http://pubs.acs.org.

■ AUTHOR INFORMATION

Corresponding Author
*Phone: (+852) 2609 6342. Fax: (+852) 2603 5057. E-mail: cfleung@cuhk.edu.hk.

■ ACKNOWLEDGMENT

This work was supported by Direct Grants for Research (Grant 2060369), Strategic Investments Scheme from The Chinese University of Hong Kong, General Research Fund (Grant CUHK-401709) from The Research Grants Council of Hong Kong and a grant from the University Grants Committee of HKSAR (Area of Excellence Scheme AoE/P-03/08).

■ REFERENCES

(1) Raj, K.; Moskowitz, R. *J. Magn. Magn. Mater.* **1990**, *85*, 233–245.
(2) Hu, A. G.; Yee, G. T.; Lin, W. B. *J. Am. Chem. Soc.* **2005**, *127*, 12486–12487.
(3) Sen, T.; Sebastianelli, A.; Bruce, I. J. *J. Am. Chem. Soc.* **2006**, *128*, 7130–7131.
(4) Martin, B. R.; Dermody, D. J.; Reiss, B. D.; Fang, M. M.; Lyon, L. A.; Natan, M. J.; Mallouk, T. E. *Adv. Mater.* **1999**, *11*, 1021–1025.
(5) Huo, L.; Li, W.; Lu, L.; Cui, H.; Xi, S.; Wang, J.; Zhao, B.; Shen, Y.; Lu, Z. *Chem. Mater.* **2000**, *12*, 790–794.
(6) Matijevic, P. E. In *Science of Ceramic Chemical Processing*; Hench, L. L., Ulrich, D. B.; Wiley: New York, 1986; p 463.
(7) Lu, A. H.; Salabas, E. L.; Schuth, F. *Angew. Chem., Int. Ed.* **2007**, *46*, 1222–1244.
(8) Jeong, U. Y.; Teng, X. W.; Wang, Y.; Yang, H.; Xia, Y. N. *Adv. Mater.* **2007**, *19*, 33–60.
(9) Laurent, S.; Forge, D.; Port, M.; Roch, A.; Robic, C.; Elst, L. V.; Muller, R. N. *Chem. Rev.* **2008**, *108*, 2064–2110.
(10) Sun, S.; Zeng, H. *J. Am. Chem. Soc.* **2002**, *124*, 8204–8205.
(11) Deng, H.; Li, X.; Peng, Q.; Wang, X.; Chen, J.; Li, Y. *Angew. Chem., Int. Ed.* **2005**, *44*, 2782–2785.
(12) Ge, J.; Hu, Y.; Biasini, M.; Beyermann, W. P.; Yin, Y. *Angew. Chem., Int. Ed.* **2007**, *46*, 4342–4345.
(13) Zhuang, J. Q.; Wu, H. M.; Yang, Y. G.; Cao, Y. C. *J. Am. Chem. Soc.* **2007**, *129*, 14166–14167.
(14) Liu, J.; Sun, Z. K.; Deng, Y.; Zou, Y.; Li, C.; Guo, X.; Xiong, L.; Gao, Y.; Li, F.; Zhao, D. Y. *Angew. Chem., Int. Ed.* **2009**, *48*, 5875–5879.
(15) Hu, F.; MacRenaris, K. W.; Waters, E. A.; Schultz-Sikma, E. A.; Eckermann, A. L.; Meade, T. J. *Chem. Commun.* **2010**, *46*, 73–75.
(16) Tang, Y.; Chen, Q. W. *Chem. Lett.* **2007**, *36*, 840–841.
(17) Geng, B. Y.; Zhan, F. M.; Jiang, H.; Guo, Y. J.; Xing, Z. J. *Chem. Commun.* **2010**, *44*, 5773–5775.
(18) Bai, F.; Wang, D. S.; Huo, Z. Y.; Chen, W.; Liu, L. P.; Liang, X.; Chen, C.; Wang, X.; Peng, Q.; Li, Y. D. *Angew. Chem., Int. Ed.* **2007**, *46*, 6650–6653.
(19) Leung, K. C.-F.; Wang, Y.-X. J.; Wang, H. H.; Xuan, S. H.; Chak, C.-P.; Cheng, C. H. K. *IEEE Trans. Nanobiosci.* **2009**, *8*, 192–198.
(20) Jia, J. C.; Yu, J. C.; Wang, Y.-X. J.; Chan, K. M. *ACS Appl. Mater. Interfaces* **2010**, *2*, 2579–2584.
(21) Zhu, Y. F.; Kockrich, E.; Ikoma, T.; Hanagata, N.; Kaskel, S. *Chem. Mater.* **2009**, *21*, 2547–2553.
(22) Tsung, C. K.; Fan, J.; Zheng, N. F.; Shi, Q. H.; Forman, A. J.; Wang, J. F.; Stucky, G. D. *Angew. Chem., Int. Ed.* **2008**, *47*, 8682–8686.
(23) Kresge, C. T.; Leonowicz, M. E.; Roth, W. J.; Vartuli, J. C.; Beck, J. S. *Nature* **1992**, *359*, 710–712.
(24) Slowing, I. I.; Trewyn, B. G.; Giri, S.; Lin, V. S. Y. *Adv. Funct. Mater.* **2007**, *17*, 1225–1236.
(25) Ying, J. Y.; Mehnert, C. P.; Wong, M. S. *Angew. Chem., Int. Ed.* **1999**, *38*, 56–77.
(26) Davis, M. E. *Nature* **2002**, *417*, 813–821.
(27) Rosenholm, J. M.; Meinander, A.; Peuhu, E.; Niemi, R.; Eriksson, J. E.; Sahlgren, C.; Linden, M. *ACS Nano* **2009**, *3*, 197–206.
(28) Lee, J. E.; Lee, N.; Kim, H.; Kim, J.; Choi, S. H.; Kim, J. H.; Kim, T.; Song, I. C.; Park, S. P.; Moon, W. K.; Hyeon, T. *J. Am. Chem. Soc.* **2010**, *132*, 552–557.
(29) Guo, S. J.; Li, D.; Zhang, L. X.; Li, J.; Wang, E. K. *Biomaterials* **2009**, *30*, 1881–1889.
(30) Lin, Y. S.; Wu, S. H.; Hung, Y.; Chou, Y. H.; Chang, C.; Lin, M. L.; Tsai, C. P.; Mou, C. Y. *Chem. Mater.* **2006**, *18*, 5170–5172.
(31) Wang, Y. X.; Hussain, S. M.; Krestin, G. P. *Eur. Radiol.* **2001**, *11*, 2319–2331.
(32) Clement, O.; Luciani, A. *Eur. Radiol.* **2004**, *14*, 1498–1507.
(33) Metz, S.; Lohr, S.; Settles, M.; Beer, A.; Woertler, K.; Rummeny, E. J.; Daldrup-Link, H. E. *Eur Radiol.* **2006**, *16*, 598–607.
(34) Alexiou, C.; Arnold, W.; Klein, R. J.; Parak, F. G.; Hulin, P.; Bergemann, C.; Erhardt, W.; Wagenpfeil, S.; Lübbe, A. S. *Cancer Res.* **2000**, *60*, 6641–6648.
(35) Cheng, K.; Peng, S.; Xu, C. J.; Sun, S. H. *J. Am. Chem. Soc.* **2009**, *131*, 10637–10644.
(36) Kim, J.; Kim, H. S.; Lee, N.; Kim, T.; Kim, H.; Yu, T.; Song, I. C.; Moon, W. K.; Hyeon, T. *Angew. Chem., Int. Ed.* **2008**, *47*, 8438–8441.
(37) Piao, Y.; Kim, J.; Na, H. B.; Kim, D.; Baek, J. S.; Ko, M. K.; Lee, J. H.; Shokouhimehr, M.; Hyeon, T. *Nat. Mater.* **2008**, *7*, 242–247.
(38) Lindig, B. A.; Rodgers, M. A. J.; Schaap, A. P. *J. Am. Chem. Soc.* **1980**, *102*, 5590–5593.
(39) Nasongkla, N.; Bey, E.; Ren, J.; Ai, H.; Khemtong, C.; Guthi, J. S.; Chin, S. F.; Sherry, A. D.; Boothman, D. A.; Gao, J. *Nano Lett.* **2006**, *6*, 2427–2430.
(40) Rieter, W. J.; Kim, J. S.; Taylor, K. M. L.; An, H.; Lin, W.; Tarrant, T.; Lin, W. *Angew. Chem., Int. Ed.* **2007**, *46*, 3680–3682.
(41) Liong, M.; Lu, J.; Kovochich, M.; Xia, T.; Ruehm, S. G.; Nel, A. E.; Tamanoi, F.; Zink, J. I. *ACS Nano* **2008**, *2*, 889–896.
(42) van Schooneveld, M. M.; Vucic, E.; Koole, R.; Zhou, Y.; Stocks, J.; Cormode, D. P.; Tang, C. Y.; Gordon, R. E.; Nicolay, K.; Meijerink, A.; Fayad, Z. A.; Mulder, W. J. M. *Nano Lett.* **2008**, *8*, 2517–2525.
(43) Kim, J.; Piao, Y.; Hyeon, T. *Chem. Soc. Rev.* **2009**, *38*, 372–390.

(44) Zhu, Y. F.; Zhao, W. R.; Chen, H. R.; Shi, J. L. *J. Phys. Chem. C* **2007**, *111*, 5281–5285.
(45) Liu, X. W.; Hu, Q. Y.; Fang, Z.; Wu, Q.; Xie, Q. B. *Langmuir* **2009**, *25*, 7244–7248.
(46) Zhong, L. S.; Hu, J. S.; Liang, H. P.; Cao, A. M.; Song, W. G.; Wan, L. J. *Adv. Mater.* **2006**, *18*, 2426–2431.
(47) Xuan, S. H.; Wang, Y.-X. J.; Leung, K. C.-F.; Shu, K. Y. *J. Phys. Chem. C* **2008**, *112*, 18804–18809.
(48) Xuan, S. H.; Wang, Y.-X. J.; Yu, J. C.; Leung, K. C.-F. *Langmuir* **2009**, *25*, 11835–11843.
(49) Chak, C.-P.; Xuan, S. H.; Mendes, P. M.; Yu, J. C.; Cheng, C. H. K.; Leung, K. C.-F. *ACS Nano* **2009**, *3*, 2129–2138.
(50) Leung, K. C.-F.; Xuan, S. H.; Lo, C.-M. *ACS Appl. Mater. Interfaces* **2009**, *1*, 2005–2012.
(51) Xuan, S. H.; Wang, Y. X. J.; Yu, J. C.; Leung, K. C.-F. *Chem. Mater.* **2009**, *21*, 5079–5087.
(52) Xuan, S. H.; Wang, F.; Wang, Y. X. J.; Yu, J. C.; Leung, K. C.-F. *J. Mater. Chem.* **2010**, *20*, 5086–5094.
(53) Chen, D. H.; Cao, L.; Huang, F. Z.; Imperia, P.; Cheng, Y. B.; Caruso, R. A. *J. Am. Chem. Soc.* **2010**, *132*, 4438–4444.
(54) Lowell, S.; Shields, J. E.; Thomas, M. A.; Thommes, M. *Characterization of Mesoporous Solids and Powders: Surface Area, Pore Size and Density*; Kluwer: London, 2004.
(55) Ge, J. P.; Hu, Y. X.; Biasini, M.; Dong, C.; Guo, J.; Beyermann, W. P.; Yin, Y. D. *Chem.—Eur. J.* **2007**, *13*, 7153–7161.
(56) Xuan, S. H.; Hao, L. Y.; Jiang, W. Q.; Gong, X. L.; Hu, Y.; Chen, Z. Y. *J. Magn. Magn. Mater.* **2007**, *308*, 210–213.
(57) Lu, Z. D.; Ye, M. M.; Li, N.; Zhong, W. W.; Yin, Y. D. *Angew. Chem., Int. Ed.* **2010**, *49*, 1862–1866.
(58) Larsen, B. A.; Haag, M. A.; Serkova, N. J.; Shroyer, K. R.; Stoldt, C. R. *Nanotechnology* **2008**, *19* (265102), 1–6.
(59) Celli, J. P.; Spring, B. Q.; Rizvi, I.; Evans, C. L.; Samkoe, K. S.; Verma, S.; Pogue, B. W.; Hasan, T. *Chem. Rev.* **2010**, *110*, 2795–2838.
(60) Lovell, J. F.; Liu, T. W. B.; Chen, J.; Zhang, G. *Chem. Rev.* **2010**, *110*, 2839–2857.
(61) Wilson, M. W.; Kerlan, R. K., Jr.; Fidelman, N. A.; Venook, A. P.; LaBerge, J. M.; Koda, J.; Gordon, R. L. *Radiology* **2004**, *230*, 287–293.